

Warner Marzocchi and Aldo Zollo (Editors)

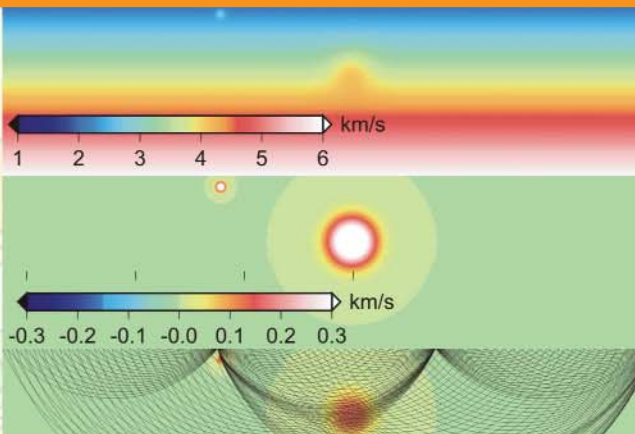
Conception, verification and application of innovative techniques to study active volcanoes

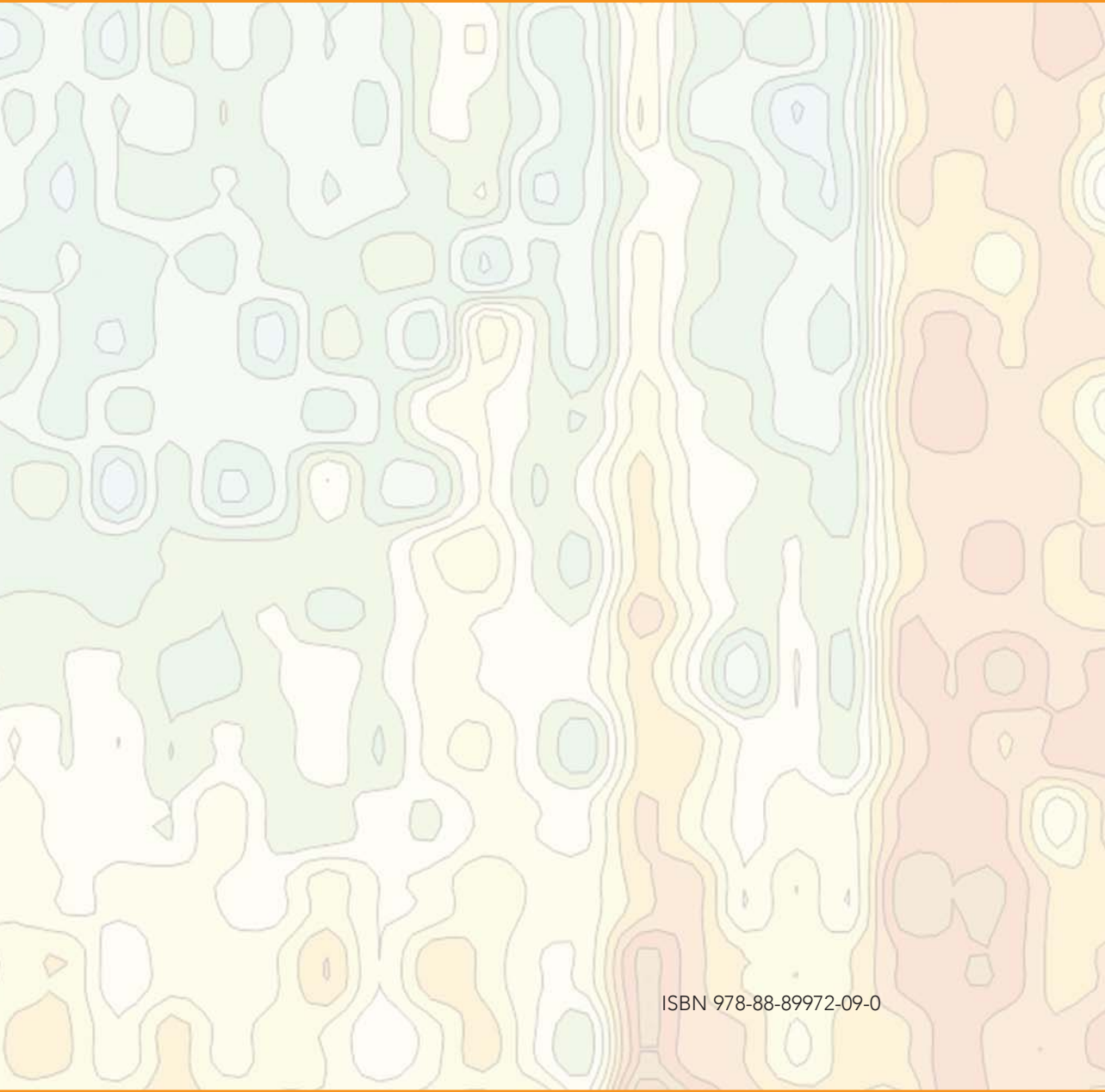


Istituto Nazionale di
Geofisica e Vulcanologia

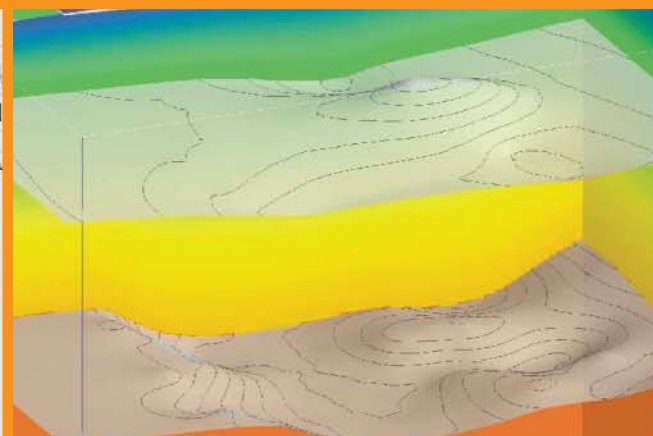
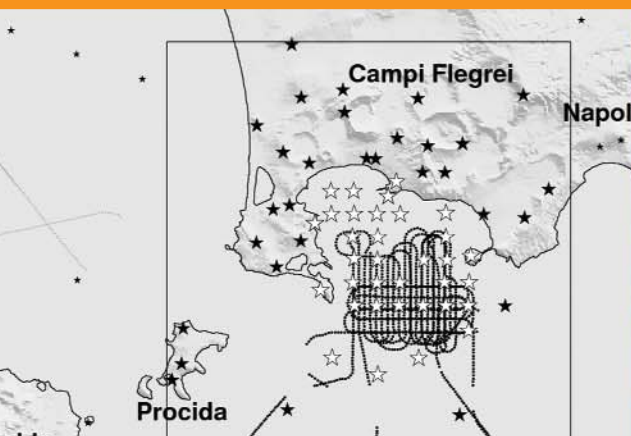


Dipartimento della
Protezione Civile





ISBN 978-88-89972-09-0



**Conception, verification and application
of innovative techniques
to study active volcanoes**

Edited by

Warner Marzocchi

Istituto Nazionale di Geofisica e Vulcanologia, Bologna, Italy

Aldo Zollo

Dipartimento di Scienze Fisiche, Università Federico II, Napoli, Italy

A cura di
Warner Marzocchi
Istituto Nazionale di Geofisica e Vulcanologia, Bologna, Italy
Aldo Zollo
Dipartimento di Scienze Fisiche, Università Federico II, Napoli, Italy

Supervisione editoriale
Sonia Sorrentino

Coordinamento editoriale
doppiavoce
www.doppiavoce.it

ISBN 978-88-89972-09-0

Copyright © 2008 Istituto Nazionale di Geofisica e Vulcanologia

Tutti i diritti riservati
È vietata ogni riproduzione

Contents

<i>Preface</i>	13
<i>Introduction</i>	15
Task 1	
ESTIMATION OF THE VOLCANIC HAZARD BASED ON PROBABILISTIC TECHNIQUES, AND ERUPTIONS FORECASTING	17
Joint inversion of geodetic data in a layered medium: a preliminary application to the Campi Flegrei caldera (Italy)	19
<i>A. Amoruso, L. Crescentini</i>	
Introduction	19
Methods	22
Data	26
Modeling	27
Conclusions	28
References	29
Dynamical and stochastic techniques	31
<i>R. Carniel, O. Jaquet, M. Tárrega</i>	
Introduction	31
The stochastic approach	31
Failure forecast method	32
Dynamical systems approach	34
Conclusions	36
References	37
ANGELA: a new package for the near-real-time inversion of geodetic data in layered media	39
<i>L. Crescentini, A. Amoruso, M. Carpentieri</i>	
Introduction	39
Configuration (requested resources)	40
Code basics	41
The ANGELA package	44
Examples	44
References	48

Tremor source location based on amplitude decay	49
<i>S. Falsaperla, G. Di Grazia, H. Langer</i>	
Introduction	49
Data	50
Method and results	53
Discussion and conclusions	55
Acknowledgments	56
References	56
Can flank instability at Stromboli volcano provide insights into precursory patterns of eruptions?	57
<i>S. Falsaperla, M. Neri, E. Pecora, S. Spampinato</i>	
Introduction	57
Data and analysis	58
Discussion and conclusions	63
Acknowledgments	65
References	65
Automatic classification of volcanic tremor using Support Vector Machine	67
<i>M. Masotti, S. Falsaperla, H. Langer, S. Spampinato, R. Campanini</i>	
Introduction	67
Data: The Case Study of Volcanic Tremor Recorded During Mt Etna's 2001 Eruption	69
Features: Averaged Spectrograms	69
Classification: Support Vector Machine	70
Results and Discussion	72
References	75
Probabilistic volcanic hazard assessment and eruption forecasting: the Bayesian Event Tree approach	77
<i>W. Marzocchi, J. Selva, L. Sandri</i>	
Purpose	77
General features of Probabilistic Volcanic Hazard Assessment (PVHA)	77
The Bayesian Event Tree (BET) applied to PVHA	81
Final Remarks on BET	87
References	88
Monitoring the source evolution of volcanic seismic swarms through a Nonstationary ETAS modeling (NETAS)	91
<i>J. Selva, W. Marzocchi, A.M. Lombardi</i>	
Purpose	91
NETAS modeling	91
Exploring the origin of volcanic seismic swarms	93
Final remarks	96
References	96

Task 2

HIGH RESOLUTION SEISMIC IMAGING OF VOLCANIC STRUCTURES 99

Combining active and passive data for velocity reconstruction 101

J. Battaglia, D. Dello Iacono, A. Zollo, J. Virieux

Introduction	101
Data	101
The tomographic inversion procedure	103
Merging of the two sets of data	103
Inversion settings	105
Tomography results	107
Resolution tests	108
Conclusion and discussion	108
Acknowledgments	110
References	110

A shear wave analysis system for semi-automatic measurements of shear wave splitting above volcanic earthquakes: descriptions and applications 113

L. Zaccarelli, F. Bianco

Introduction	113
Volcanic stress monitoring	114
SPY: Splitting Parameter Yield	114
Applications	118
Conclusions	123
References	123

Converted phases analysis of the Campi Flegrei caldera using active and passive seismic data 125

T.M. Blacic, D. Latorre, J. Virieux

Introduction	125
Methods	126
Data	128
Analysis of converted phase focusing	130
Discussion and conclusions	133
Acknowledgments	136
References	136

Seismic wave simulation in Campi Flegrei Caldera based upon Spectral Element Methods 137

E. Casarotti, A. Piersanti, J. Tromp

Introduction	137
Methods	137
Modelling	146
Discussion and conclusion	157
References	157

Methodological advances in source and attenuation studies from the inversion of rise times of P pulses recorded at a local scale	161
<i>S. de Lorenzo, E. Boschi, M. Filippucci, E. Giampiccolo, D. Patanè</i>	
Preface	161
Inversion technique	161
Data analysis	163
Data inversion	164
Fault plane resolution and a posteriori validation of results	166
Application to Mt. Etna microearthquakes	167
References	168
QP and QS of Campi Flegrei from the inversion of rayleigh waves recorded during the SERAPIS project	169
<i>S. de Lorenzo, A. Zollo, M. Trabace, M. Vassallo</i>	
Summary	169
Data analysis	169
Data inversion	174
Conclusion	180
References	180
Multi-scale decomposition of velocity structure and application to first-arrival travel-time tomography	181
<i>M. Delost, J. Virieux, S. Operto</i>	
Introduction	181
Wavelet Transformation	183
Travel-time tomography	183
Synthetic examples	186
Resolution analysis for defining the binary M operator	188
Application to a synthetic real date configuration	189
Conclusion	191
References	192
An EGF technique to infer the rupture velocity history of a small earthquake: a possible solution to the tradeoff among Q and source parameters	195
<i>M. Filippucci, S. de Lorenzo, E. Boschi</i>	
Introduction	195
The technique	195
Testing the EGF technique on synthetic seismograms	198
Testing the EGF technique on real seismograms	202
References	205
Fresnel or finite frequency approach	207
<i>S. Gautier, G. Nolet, J. Virieux</i>	
Methodology	209
Application to the western part of the Corinth rift	211

Results	214
Discussion and conclusion	216
Acknowledgments	217
References	218
Elastic full waveform inversion in the frequency domain	221
<i>C. Gélis, J. Virieux, S. Operto</i>	
Introduction	221
Frequency-domain full-waveform inversion	222
Simple canonical example	224
Construction of a 2D profile from the 3D SERAPIS experiment	225
Perspective and conclusions	229
Acknowledgments	230
References	231
Numerical simulation of seismic experiments in volcanic areas: development of a technique based on the Pseudo-spectral Fourier method and its application to the build up of synthetic data sets for the Campi Flegrei area	233
<i>P. Klin, E. Priolo</i>	
Introduction	233
Method	234
Modelling	242
Discussion and conclusion	246
References	246
Converted phases analysis for passive/active seismic data	249
<i>D. Latorre, T. Blacic, J. Virieux, T. Monfret</i>	
Method	251
Discussion and conclusion	257
Acknowledgments	258
References	258
Seismic scatterer imaging using shot array beamforming: method and application to the Campi Flegrei caldera	261
<i>N. Maercklin</i>	
Introduction	261
Imaging method	262
Application to the Campi Flegrei caldera	264
Discussion and conclusions	266
References	266
Analysis of PS-to-PP amplitude ratios for seismic reflector characterisation: method and application	269
<i>N. Maercklin, A. Zollo</i>	
Introduction	269

Analysis method	270
Application to the Campi Flegrei caldera	274
Discussion and conclusions	278
References	279
Iterative tomographic analysis based on automatic refined picking	281
<i>C. Satriano, A. Zollo, C. Rowe</i>	
Introduction	281
Picking refinement based on cross-correlation	283
Iterative Tomographic Imaging	285
Application to the active seismic data of the SERAPIS experiment	286
Discussion and conclusions	291
References	293
Acoustic full waveform inversion in the frequency domain	295
<i>F. Sourbier, S. Operto, J. Virieux</i>	
Introduction	295
Frequency-domain finite-difference waveform modelling	297
Frequency-domain full-waveform inversion	298
Perspective and conclusions	306
Acknowledgments	307
References	307
Development of a multi-phase dynamic ray-tracing code	309
<i>T.A. Stabile, R. De Matteis, A. Zollo</i>	
Introduction	309
Method	310
Method validation	313
Structure of the Comrad.f code	316
Conclusions	318
References	319
Pore pressure prediction based on passive seismic and rock physics modeling	321
<i>T. Vanorio, J. Virieux, D. Latorre</i>	
Introduction	321
Geophysical outline of the area	322
Methods	324
Results	331
Conclusion and perspectives	332
Acknowledgments	333
References	334

Depth and morphology of reflectors from the 2-D non-linear inversion of arrival-time and waveform semblance data: method and applications to synthetic data	337
<i>M. Vassallo, A. Zollo</i>	
Introduction	337
Method	338
Synthetic data modelling	340
Discussion and conclusion	344
References	347
Converted phase identification and retrieval of V_p/V_s ratios from move-out reflection analysis: application to the Campi Flegrei caldera	349
<i>M. Vassallo, A. Zollo, D. Dello Iacono, N. Maercklin, J. Virieux</i>	
Introduction	349
Method	350
Application to a synthetic dataset	351
Application to the SERAPIS data	353
Conclusion	357
References	359
Task 3	
REAL TIME OBSERVATIONS AND MEASUREMENTS	361
PLINIO: an interactive web interface for seismic monitoring of Neapolitan volcanoes	363
<i>L. D'Auria, R. Curciotti, M. Martini, G. Borriello, W. De Cesare, F. Giudicepietro, P. Ricciolino, G. Scarpato</i>	
Introduction	363
General overview of PLINIO	363
Real-time earthworm processing and WBSM database	364
Manual processing and GeoVes database	366
PHP interface and JpGraph libraries	366
Example queries	369
References	374
A unified 3D velocity model for the Neapolitan volcanic areas	375
<i>L. D'Auria, M. Martini, A. Esposito, P. Ricciolino, F. Giudicepietro</i>	
Introduction	375
Starting velocity models	375
Unification of velocity models	381
Relocation of seismic events	385
Conclusions	388
Acknowledgments	389
References	389

RS-485 interface for external use of the GPS receiver of the Kinometrics® dataloggers	391
<i>S. Guardato, G. Iannaccone</i>	
Summary	391
Functioning principles	391
Interface description	393
The datalogger-side board	394
The GPS receiver-side board	396
Electrical interconnections	398
References	398
Automatic analysis of seismic data by using Neural Networks: applications to Italian volcanoes	399
<i>F. Giudicepietro, A. Esposito, L. D'Auria, M. Martini, S. Scarpetta</i>	
Introduction	399
Neural Networks	400
Feature extraction stage	404
Application areas and results	405
References	414
CUMAS (Cabled Underwater Module for Acquisition of Seismological data): a new seafloor module for geohazard monitoring of the Campi Flegrei volcanic area	417
<i>G. Iannaccone, S. Guardato, M. Vassallo, L. Beranzoli</i>	
Introduction	417
The features of CUMAS	418
Technical characteristics of the buoy	422
Power requirements	422
Expected results	424
References	425
Use of Forward Looking InfraRed thermal cameras at active volcanoes	427
<i>L. Lodato, L. Spampinato, A.J.L. Harris, J. Dehn, M.R. James, E. Pecora, E. Biale, A. Curcuruto</i>	
Introduction	427
Thermal camera installation at La Fossa crater, Vulcano (Aeolian Archipelago)	428
References	434
A multiparametric low power digitizer: project and results	435
<i>M. Orazzi, R. Peluso, A. Caputo, M. Capello, C. Buonocunto, M. Martini</i>	
Introduction	435
System architecture and project	436
The main connection board	442
Firmware description	443
Conclusions and results	452

Thermal gradiometer's array: mechanical and electrical design and first field test results	461
<i>G. Romeo, S. Bello, P. Benedetti, M. Mari, G. Urbini</i>	
1-wire design	461
Gradiometer prototypes: electrical and logic design	461
Mechanical design	463
Gradiometers connection	466
Data logging	466
Hardware implementation	469
Field tests	473
References	473
Thermal gradiometer: purposes, design and performance	475
<i>G. Romeo, G. Chiodini, F. Pongetti</i>	
Introduction	475
Temperature measurements	475
Thermal gradiometer assembly	477
1-wire thermometers	477
Prototype test	479
References	480
The permanent thermal infrared network for the monitoring of hydrothermal activity at the Solfatara and Vesuvius volcanoes	483
<i>G. Vilaro, G. Chiodini, V. Augusti, D. Granieri, S. Caliro, C. Minopoli, C. Terranova</i>	
Introduction	483
Experiment design and system development	484
The TIR remote monitoring station	485
The TIR acquired scenes	487
The portable TIR monitoring station	489
Analysis of the Solfatara TIR image series	490
Conclusions	495
Acknowledgments	496
References	496

Use of Forward Looking InfraRed thermal cameras at active volcanoes

L. Lodato¹, L. Spampinato¹, A.J.L. Harris², J. Dehn³, M.R. James⁴,
E. Pecora¹, E. Biale¹, A. Curcuruto⁵

1 Istituto Nazionale di Geofisica e Vulcanologia, Sezione di Catania, Catania, Italy

2 HIGP/SOEST, University of Hawaii, Honolulu, Hawaii, USA

3 University of Alaska Fairbanks, Alaska, USA

4 Environmental Science Department, Institute of Environmental and Natural Sciences, Lancaster University, Lancaster, United Kingdom

5 Department of Engineering, University of Catania, Catania, Italy

INTRODUCTION

Nowadays, thermal imaging has become a common remote sensing tool for monitoring active volcanoes. The study of temperature variations within open-conduit systems, at eruptive fissures, active vents, domes, lava lakes, lava fields and other volcanic features has proven fundamental to better understand volcanic system behaviour over the short and long terms (Harris and Stevenson, 1997; Oppenheimer and Yirgu, 2002; Calvari et al., 2004; Wadge et al., 2006). At INGV Catania Section, thermal imaging has been applied at Mt Etna, Stromboli, Vulcano and Panarea since 2001.

The instruments used are thermal cameras manufactured by FLIR (Forward Looking InfraRed) and consist in uncooled bolometers that are sensitive within 7.5 and 13 μ wavelengths. Thermal cameras are based on the capability to detect radiation emitted by bodies according to Planck's Law.

In particular, the camera we used is a FLIR thermal camera A 40 M Ethernet with a focal plane array uncooled bolometer (320 x 240 pixels), and a spectral range between 7.5 and 13 micrometers (Figure 1.). It has a standard optics 24° with spatial resolution (IFOV, instantaneous field of view) of 1.3 mrad, a horizontal view of 24° and a vertical view of 18°. This camera has also been equipped with optional filter to measure temperature values up to 1500°C with the possibility of setting up different temperature ranges.

The thermal camera can record and transfer in real time via wi-fi radiometric frames in JPG format of the observed eruptive activity according to some environmental parameters, such as external temperature, air humidity and emissivity and allows the vision of volcanic activity both day and night.

Temperature range varies between 0 e 500° C and the emissivity value $\epsilon = 1$. To correct the temperature of all pixels from the atmospheric attenuation



Fig. 1. Thermal camera FLIR A 40 M.

effects, we considered atmospheric parameters, such as air temperature and air humidity, in addition to the introduction of the path length (400 m) in the camera software. In fact, the radiations detected by the FLIR thermal cameras, that work in the spectral band between 7.5 e 13 μm , are affected by the absorption factor from the water spectrum, which is predominant in this band; particularly at La Fossa crater where the water content in the fumaroles is higher than the other gas species.

Because of the necessity to correct the radiometric data from the atmospheric factors in real-time, we installed a meteorological station able to interface with the camera to provide atmospheric parameters for the auto-calibration.

THERMAL CAMERA INSTALLATION AT LA FOSSA CRATER, VULCANO (AEOLIAN ARCHIPELAGO)

Between 18 and 20 July 2005, L. Lodato and L. Spampinato from INGV-Catania, A.J.L. Harris from SOEST, University of Hawaii, and J. Dehn University of Fairbank, Alaska, carried out two days of thermal measurements at La Fossa crater (Vulcano Island) (Figure 2).

The survey had a dual purpose:

1. to continue thermal measurements at fumaroles performed by Harris since 1994, using infrared handheld thermometers and thermocouples (Harris and Stevenson, 1997; Harris and Maciejewski, 2000);
2. to repeat the same measurements by using FLIR thermal cameras, to test their ability for monitoring La Fossa's fumarole field.

Measurements involved four FLIR thermal cameras imaging the Lower fumarolic zone (Figure 2). Cameras were aligned in a NE-SW direction on the opposite inner flank (southern) of the crater, at distances of 50, 100, 200 and

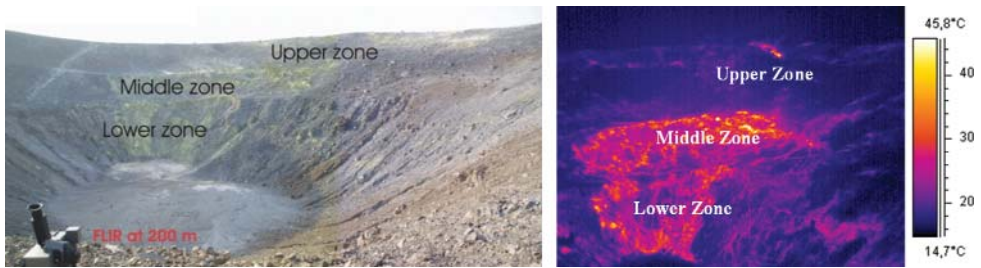


Fig. 2. Photo and thermal imaging of La Fossa's fumarole field taken from the opposite inner flank of the crater. Three main fumarolic zones, Lower, Middle and Upper zone are distinguished according to Harris and Maciejewski (2000).

400 m from the Lower zone. Thermal cameras were tripod mounted and synchronized with GMT time. GPS points for each measurement station were recorded.

For applying thermal cameras, internal calibration for atmospheric corrections of temperature for all pixels, air temperature and relative humidity were measured in situ using handheld hygrometers. Emissivity used was 0.9751, according to Harris and Maciejewski (2000) and the acquisition frequency chosen was 10 seconds.

Additionally, a 12-degree lens was also applied to the 400 m distant FLIR. This lens increased the camera magnification by a factor of two, corresponding to half of the real pathlength (Harris et al., submitted to Bulletin of Volcanology in 2007).

During the second day of measurements, a fifth thermal camera located at ~ 350 m distance from the Lower zone was used. The instrument was a FLIR A 40 M thermal camera, the kind used at Mt Etna and Stromboli permanent stations.

The analysis of thermal images collected during the entire survey proved the reliability of thermal cameras for monitoring La Fossa fumarole field. This provided us the input to develop a methodology to improve thermal data collection and the monitoring system at Vulcano fumaroles.

Indeed, the opportunity to install a permanent thermal camera could have enabled us the possibility to:

1. record thermal images in continuous and real-time,
2. acquire images with the same easily comparable geometry,
3. control the whole system from INGV Catania main site.

Thermal camera installation

A year later, in June 2006, an A 40 FLIR thermal camera was installed at almost the same 400 m distant site from the Lower zone, chosen during the

thermal survey of the previous year. For this distance, the effective pixel size resulted $\sim 50 \times 50$ cm. This location allowed imaging the Lower, Middle and Upper zone, and part of the fumaroles located at the northeastern crater rim (Figure 3).

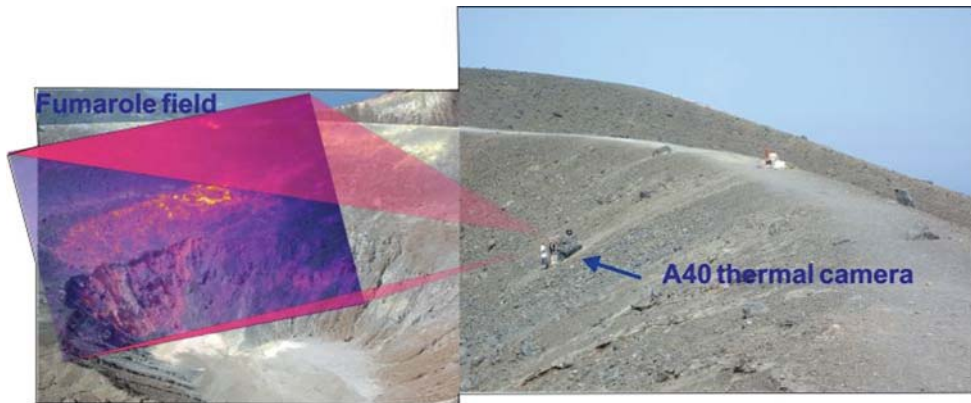


Fig. 3. Photo of La Fossa inner crater taken from the southwestern crater rim showing the A 40 location. The overlapped thermal image represents the camera field of view.

The thermal camera began acquisition at the end of September 2006 with a frequency of 30 minutes.

The installation occurred in two main phases:

- *First phase:* thermal camera installation.
- *Second phase:* weather station installation and mainboard for the interface between the thermal camera and the weather station.

First phase: thermal camera installation

In June 2006, thanks to the support of the helicopter of DPC (Dipartimento di Protezione Civile Nazionale), the thermal camera station was installed (Figure 4). This comprised an A 40 M FLIR thermal camera, photovoltaic power system and wi-fi system for radiometric data transmission.

The A 40 camera was located within a polycarbonate box supported by a steel inox structure, whereas the battery was put into a Gewiss resin box (Figure 5). To protect the thermal camera lens from alteration by volcanic gases, the polycarbonate box was equipped with an additional germanium lens. Moreover, due to high air temperatures occurring during Summer (temperatures $> 60^{\circ}$ C), the thermal station was equipped with a chronothermostat.



Fig. 4. Photo taken from La Fossa southern crater rim 24 June 2006. Helicopter of DPC Nazionale transporting the thermal station components.



Fig. 5. Polycarbonate box containing the A 40 M FLIR thermal camera.

Radiometric data transfer and thermal camera remote control are controlled by an access point equipped with a serial and Ethernet connection.

The serial connection creates the interface between the thermal camera and the weather station, while the Ethernet connection links the thermal camera with the access point.

Radiometric data are transferred by wi-fi to Lipari (INGV Catania) site, sent to Catania (CUAD, Centro Unificato Acquisizione Dati, Catania) by Garr network (2 Mbps), where they are stored on a personal computer and analyzed in real-time by IDL software. In detail, the access point, located within the Gewiss resin box, communicates with the Lipari system through a directional antenna (Figure 6).



Fig. 6. Directional antenna for wi-fi data transmission to Lipari Island.

At Lipari (Osservatorio della Marina), another access point (Alvarion) was installed for the acquisition of radiometric and atmospheric data transmitted by the thermal station in Vulcano.

The feeding system comprised two photovoltaic Kyocera panels with a steel inox structure, linked to a charge regulator through an electric cable (Figures 7a,b).

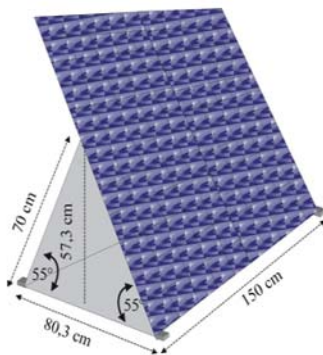


Fig. 7. Left (a), Kyocera photovoltaic panel project; right (b), photo showing the photovoltaic panel installation.

Energy necessary to supply the thermal station was calculated by considering that:

- the thermal camera has to work 24 hours per day,
- an average of three hours of sun light taking into account Winter and Summer,
- without sun light, the battery has almost two days of autonomy, and
- the whole system needs an average of 550 W/day.

Second phase: weather station installation

In January 2007, to apply corrections for the atmospheric parameters within the thermal camera internal software in real-time, a weather station close to the thermal camera was installed. The remote control, the atmospheric parameter acquisition and the interface between the A 40 and the weather station is managed by a mainboard.

The weather station is a La Lacrosse WS 2305 (Figure 8) provided of a hygrometer, anemometer, rain gauge and a temperature sensor.

The microcontroller used to create the interface between the components of the entire system (Figure 8), is a Microchip Pic (Peripheral Interface Controller) 18F258. In particular, the microcontroller reads the atmospheric parameters recorded by the weather station and sends them to the access point. Additionally, it periodically sends values of air temperature and relative humidity to the thermal camera for the autocalibration (Figure 9).

The whole system was tested in Catania before the installation.



Fig. 8. La Lacrosse WS 2305 weather station.

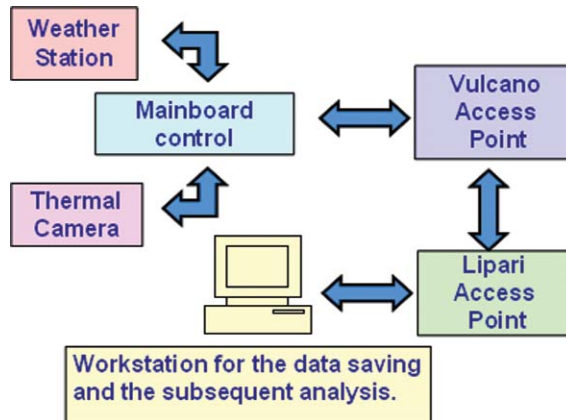


Fig. 9. Block diagram of the system.

Future development

During a survey two months after the installation of the station, we observed that it shows very clear corrosion traces due to highly corrosive gases emitted by Vulcano, even more marked than those observed at Stromboli stations (Figure 10).

For this reason, we are performing a study to carry out special protection for future installations in this kind of environment.

The polycarbonate case well preserved the thermal camera from the acid gas corrosions.

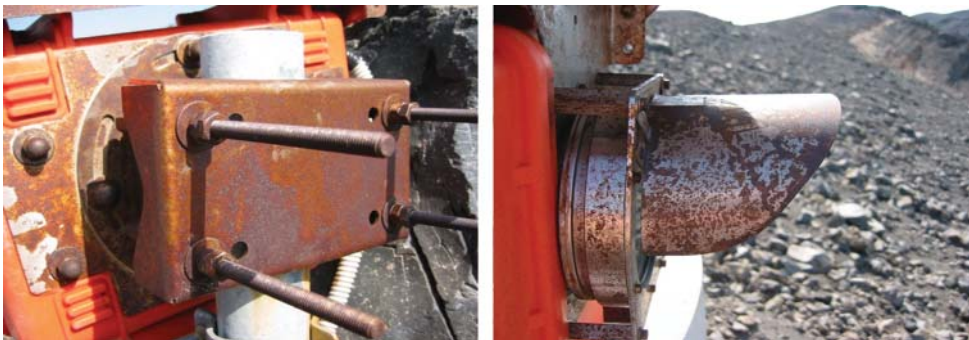


Fig. 10. Gas corrosion effects at Vulcano station.

REFERENCES

- Calvari, S., Lodato, L., Spampinato, L., 2004. Monitoring active volcanoes using a hand-held thermal camera. *Thermosense XXVI-SPIE, The International Society for Optical Engineering* 5405, 199-209, DOI: 10.1117/12.547497.
- Harris, A.J.L., Stevenson, D.S., 1997. Magma budgets and steady-state activity of Vulcano and Stromboli volcanoes. *Geophys Res Lett* 24:1043-1046.
- Harris A.J.L., Maciejewski A.J.H., 2000. Thermal survey's of the Vulcano Fossa fumarole field 1994-1999: evidence for fumarole migration and sealing. *J Volcanol Geotherm Res* 102:119-147.
- Harris, A.J.L., Lodato L., Dehn J., Spampinato L., 2007. Thermal Characterization of Fumarole Fields. Submitted to *Bulletin of Volcanology* in 2007.
- Oppenheimer, C., Yirgu, G., 2002. Thermal imaging of an active lava lake: Erta 'Ale volcano, Ethiopia. *Int. J. Remote Sens.* 23(22), 4777-4782.
- Wadge, G., Macfarlane, D.G., James, M.R., Odbert, H.M., Applegarth, L.J., Pinkerton, H., Duncan, A.R., Loughlin, S.C., Strutt, M., Ryan, G., Dunkley, P., 2006. Imaging a Growing Lava Dome with a Portable Radar. *EOS, Trans. AGU* 87, 23.